

Rapid proton capture on accreting neutron stars – effects of uncertainty in the nuclear process

O. Koike¹, M. Hashimoto¹, K. Arai², and S. Wanajo³

¹ Department of Physics, Kyushu University, Ropponmatsu, Fukuoka 810-8560, Japan

² Department of Physics, Kumamoto University, Kurokami, Kumamoto 860-8555, Japan

³ Division of Theoretical Astrophysics, National Astronomical Observatory, Mitaka, Tokyo 181-8588, Japan

Received 19 August 1998 / Accepted 2 October 1998

Abstract. The rapid proton capture process on accreting neutron stars is investigated with the use of the current nuclear data and extended nuclear reaction networks. A simple but crucial model is adopted to investigate the detailed nucleosynthesis during the burst: the plane parallel (one zone) model. Compared with the results of Hanawa et al. (1983), significant differences are found. The peak temperature becomes higher due to the rapid break out from the hot CNO cycle. The amount of the fuel left after the burst depends on the still uncertain Q -values of (p, γ) reactions for nuclei like ^{68}Se . It is also demonstrated that the uncertainties in the nuclear data should influence significantly the profile of the light curve in the burst models.

Key words: nuclear reactions, nucleosynthesis, abundances – stars: neutron – X-rays: bursts

1. Introduction

It has been widely accepted that type I X-ray bursts from low mass X-ray binaries (LMXBs) are due to thermonuclear run-aways in accreted materials on the surface of neutron stars (e.g. Taam 1985, Lewin et al. 1993, Bildsten 1998). Detailed evolutionary calculations have been performed taking into account the nuclear process during the flash (e.g. Fujimoto et al. 1987, Taam et al. 1996). Recent observations of LMXBs by the Rossi X-Ray Timing Explorer have revealed several important new features related to X-ray bursts. For example, a burst from 4U 1728–34 would be produced by the spin modulation of a localized thermonuclear hot spot on the surface of a rotating neutron star with a millisecond period (Strohmayer et al. 1998) where kilohertz quasi-periodic oscillations (QPOs) are discussed related to the models to constrain the mass and radius of the neutron star. Furthermore, analyzing the burst observation of Cyg X-2, Smale (1998) suggested super-Eddington bursts which resulted from the photospheric expansion. Also he inferred the source distance using an assumed neutron star mass as high as $2 M_{\odot}$ which seems to be consistent with an estimate of Kaaret et al. (1997) for different observations of QPOs. However, the supernova 1987A could have produced a black hole of $\sim 1.5 M_{\odot}$

(Brown & Bethe 1994) which could not be compatible with the above estimates. Therefore, we can say that recent observations of X-ray burst phenomena provide new challenges to both the model of bursts and the theory of neutron star structure.

On the other hand, many nuclear data have been revised and accumulated in these years, some of which may affect the modeling of X-ray bursts. The nuclear process in the proton rich environments was investigated in detail by Wallace & Woosley (1981) where the rapid proton capture process (rp-process) was first proposed. Recently the rp-process has been investigated extensively from a point of the fundamental nuclear process (see e.g. Wormer et al. 1994, Rembges et al. 1997, Schatz et al. 1998). In those series of the papers, they investigated nuclear flows under the condition of constant temperature and density or the assumption of “adiabatic expansion” to see the effects of uncertainties of nuclear physics. Among all, Schatz et al. (1998) analyzed the relation between the nuclear data and the rp-process which would occur at extreme temperature and density conditions with the use of a large nuclear reaction network. However, more plausible models which simulate the thermonuclear flash would be very necessary to examine how the revised nuclear data affect actually physical conditions during the flash. Unfortunately, at present it is difficult to perform multi-dimensional hydrodynamical calculations which include both general relativity in the strong field and the complete nuclear reaction network. Therefore, a simple but crucial model which represents a thermonuclear flash phase is very useful to extract the effects of physical inputs on the flash.

In the spirit of the one zone model of constant pressure, explosive nucleosynthesis (Hashimoto et al. 1983) and the rp-process (Hanawa et al. 1983, hereafter HSH) were investigated in detail with the use of large networks. In the calculations of the rp-process, they have shown clearly that not only the nucleosynthesis proceeds appreciably beyond ^{56}Ni but also appreciable amounts of the nuclear fuel of hydrogen and helium are left if the peak temperature exceeds 10^9 K for the pressure of $P \gtrsim 3 \cdot 10^{22}$ dyn cm $^{-2}$; it was suggested that the unburnt fuel may be responsible for the X-ray bursts at 10 minute interval. Using their approximate network, Fujimoto et al. (1987) investigated X-ray bursts in detail with the evolutionary calculations of an accreting neutron star. Unfortunately, HSH did not

Send offprint requests to: M. Hashimoto

discuss how the uncertainties of the initial abundances and the nuclear data affect the thermonuclear history during the flash; since then there have been many revisions of the nuclear data related to the rp-process, it should be worth while investigating the effects of the new data on the flash. For example, uncertainties of Q -values of the proton capture must influence the path in the nuclear chart and therefore the time scale of the burst (see e.g. Schatz et al. 1998), because the path of the rp-process is almost along the proton drip line after the leakage from the hot CNO (HCNO) cycle.

In the present paper, we will investigate the thermonuclear flash with the use of an extended network up to ^{94}Kr based on the network constructed by Hashimoto & Arai (1985) which will be coupled to the thermodynamical equation for the flash as was done by HSH. In our calculation, we will use the up-to-date nuclear data and other physical inputs like screening factors. Then, by considering that the nuclear process for the rp-process has been examined by Wormer et al. (1994) and Schatz et al. (1998) in detail, special attention will be paid rather to see the effects of the uncertainty of nuclear data on thermal histories of the shell flash related to the fuel left unburnt.

In Sect. 2, we describe a type I X-ray burst model which presents characteristic features of the thermonuclear flash in accreting neutron stars. Physical data incorporated in our network are explained in Sect. 3. Computational results for the rp-process during the flash are presented in Sect. 4 in connection with uncertainties of the nuclear data. Discussion and conclusions are given in Sect. 5.

2. Type I X-ray burst model

As a type I X-ray burst model for the rp-process, we adopt a plane parallel approximation by Fujimoto et al. (1981). This model is reasonable enough to investigate the nuclear process during the shell flash if we assume that physical quantities are averaged over the accumulated layers, hydrostatic equilibrium is maintained, and the configuration is spherically symmetric. In fact, Hashimoto et al. 1983, and HSH have performed the calculation of the nucleosynthesis under these assumptions. Let us summarize the formulation of the model for the following discussion.

A hydrostatic equilibrium equation to determine the structure of the accreting neutron star is written as follows:

$$\frac{dP}{dM_r} = -\frac{GM_r}{4\pi r^4} \left(1 - \frac{2GM_r}{rc^2}\right)^{-1/2}. \quad (1)$$

Here, P is the pressure and M_r is the rest mass contained interior to the radius r . For a plane parallel configuration which can be legitimate as far as the ratio of the radius to the pressure scale height is as large as 10^3 , the column mass density Σ and the surface gravity g_s are introduced. Using the total gravitational mass M_t , the accreted proper mass ΔM and the radius R at the surface, they are defined as follows:

$$\Sigma = \frac{\Delta M}{4\pi R^2} = 1.6 \cdot 10^{20} \frac{\Delta M/M_\odot}{(R/10 \text{ km})^2} \text{ g cm}^{-2}, \quad (2)$$

$$g_s = \frac{GM_t}{R^2} V = 1.3 \cdot 10^{14} \frac{M_t/M_\odot}{(R/10 \text{ km})^2} V \text{ cm s}^{-2}, \quad (3)$$

where $V = (1 - 2GM_t/Rc^2)^{-1/2}$ is the general relativistic correction factor of Schwarzschild metric. We have $V = 1.3$ and $\log g_s = 14.4$ for a model with $M_t = 1.4M_\odot$ and $R = 10 \text{ km}$. The amount of accreted matter $\Delta M/M_\odot$ can be estimated from 10^{-13} to 10^{-11} (Fujimoto et al. 1987).

Eq. (1) is integrated and reduced to be a constant pressure if we adopt a plane parallel approximation:

$$P = 10^{22} g_{14} \Sigma_8 \text{ dyn cm}^{-2}, \quad (4)$$

where $g_{14} = g_s/10^{14} \text{ cm s}^{-2}$ and $\Sigma_8 = \Sigma/10^8 \text{ g cm}^{-2}$ are considered to be parameters which are assumed to be constant during the burst. For example, around the ignition, we have $\Sigma_8 \sim 2.5$ for $g_{14} \sim 1$ with the helium mass fraction $X(^4\text{He}) \sim 0.25$ and that of CNO elements $Z_{\text{CNO}} \sim 0.02$ (Fujimoto et al. 1987).

The energy equation is written as

$$c_p \frac{dT}{dt} = \varepsilon_n - \varepsilon_\nu - \varepsilon_{\text{rad}}, \quad (5)$$

where T is the temperature, c_p is the specific heat at the constant pressure, ε_n is the nuclear energy generation rate, and ε_ν is the neutrino energy loss rate by β -decays associated with the nuclear reactions. The neutrino loss due to the direct interactions between electrons and neutrinos can be neglected during the flash. Radiative energy loss rate ε_{rad} is approximated by

$$\begin{aligned} \varepsilon_{\text{rad}} &= \frac{4ac T^4}{3\kappa \Sigma^2} \\ &= 1.5 \cdot 10^{17} T_9^4 (1 + 2.2 T_9) \left(\frac{\mu_e}{2}\right) \Sigma_8^{-2} \text{ ergs g}^{-1} \text{ s}^{-1}, \end{aligned} \quad (6)$$

where $T_9 = T/10^9 \text{ K}$, a is the radiation density constant and μ_e is the mean molecular weight per electron which in the early phase of the flash would be approximated to be $\mu_e = 2/(1 + X)$ with the hydrogen mass fraction X , when hydrogen is dominant. For opacity κ , the Compton scattering opacity is adopted (e.g. Ebisuzaki et al. 1983).

The nuclear reaction network has been coupled to the thermodynamical equations through ε_n . The rate equations of abundance are written as follows:

$$\begin{aligned} \frac{dy_0}{dt} &= - \sum_{\substack{lm\dots n \\ 01\dots k}} \lambda_{01\dots k}^{lm\dots n} y_0 y_1 \cdots y_k \\ &+ \sum_{\substack{lm\dots n \\ 01\dots k}} \lambda_{lm\dots n}^{01\dots k} y_l y_m \cdots y_n. \end{aligned} \quad (7)$$

Here the first and second terms account for the destruction and production, respectively, of the 0-th abundance y_0 and $\lambda_{ij\dots k}^{lm\dots n}$ expresses the rate of reaction or decay $i + j + \cdots + k \rightarrow l + m + \cdots + n$, where $i \cdots n$ denote the species of particles concerned: nucleus, neutron, proton, electron, positron, neutrino, antineutrino, and photon.

Once a set of parameters (P, g) or (P, Σ) is specified, using the initial values of temperature and abundances, we can get density and other thermodynamical quantities for the next time step

Table 1. Elements included in the nuclear reaction network.

| elements | A | elements | A | elements | A |
|----------|-------|----------|-------|----------|-------|
| H | 1–3 | Al | 22–31 | Mn | 46–64 |
| He | 3–6 | Si | 24–34 | Fe | 47–65 |
| Li | 6–8 | P | 27–38 | Co | 50–66 |
| Be | 7–10 | S | 28–42 | Ni | 51–68 |
| B | 8–12 | Cl | 31–45 | Cu | 56–71 |
| C | 11–14 | Ar | 32–48 | Zn | 57–74 |
| N | 12–15 | K | 35–49 | Ga | 60–77 |
| O | 14–20 | Ca | 36–50 | Ge | 61–80 |
| F | 17–22 | Sc | 39–51 | As | 64–83 |
| Ne | 17–24 | Ti | 40–53 | Se | 65–84 |
| Na | 20–27 | V | 43–55 | Br | 68–89 |
| Mg | 20–29 | Cr | 44–58 | Kr | 68–94 |

from the equation of state. Here the total pressure P consisted of the contributions from partially relativistic and/or degenerate electrons and positrons in thermal equilibrium, ions, radiation, and the Coulomb interactions (Slattery et al. 1982, Yakovlev & Shalybkov 1989):

$$P = P_e + P_{\text{ion}} + P_{\text{rad}} + P_{\text{Coul}}. \quad (8)$$

We note that in the calculation of c_p , we have taken into account the effects of non-ideal gas as P . The maximum temperature T_{max} can be estimated from $P = P_{\text{rad}}$:

$$T_{\text{max}} = 2.5 \cdot 10^9 \left(\frac{P}{10^{23} \text{ dyn cm}^{-2}} \right)^{1/4} \text{ K}. \quad (9)$$

Here, the region is assumed to be radiation dominated around the peak of the flash. HSH have examined the shell flashes for $22 \lesssim \log P \lesssim 23$ and $13.8 \lesssim \log g_s \lesssim 15.0$; During the shell flash, the peak temperature in units of 10^9 K ranges from $T_{9p} \simeq 1$ –2 and the corresponding density ranges from $\rho \simeq 5 \cdot 10^5$ – $2 \cdot 10^6$ g cm $^{-3}$.

3. Thermonuclear reaction rates, physical inputs and initial conditions

In the investigation by HSH, the nuclear reaction network included 274 nuclides from ^1H to ^{84}Kr . The nuclear reactions are assumed to proceed through (p, γ) , (α, γ) , $(3\alpha, \gamma)$, (α, p) , and their reverse reactions, and β^+ -decays. Considerable progress in nuclear physics near the proton drip line has been reported in these 10 years (e.g. see the review by Schatz et al. 1998). We have extended the nuclear reaction network to include 463 nuclides in which the reaction rates in the network developed by Hashimoto & Arai (1985) have been replaced by the current ones (see Table 1). Our previous network (hereafter, HA85) which corresponds to cases A and B in Table 2 has used the compilation of the reaction rates by Fowler et al. (1975), Woosley et al. (1975, 1978), Wallace & Woosley (1981), Harris et al. (1983), Caughlan et al. (1985). The elements included in our new reaction network are shown in Table 1 which corresponds to case C in Table 2. For completeness, we have also included the neutron

Table 2. Half lives and Q -values of the (p, γ) reactions in units of keV which determine the waiting point during the shell flash and the final products.

| Waiting point | case A | | case B | | case C | |
|------------------|-----------|----------------|-----------|----------------|-----------|----------------|
| | $t_{1/2}$ | $Q(p, \gamma)$ | $t_{1/2}$ | $Q(p, \gamma)$ | $t_{1/2}$ | $Q(p, \gamma)$ |
| ^{56}Ni | 6.1 d | 691 | 6.1 d | 767 | 6.1 d | 767 |
| ^{64}Ge | 64 s | 9 | 64 s | 129 | 64 s | 169 |
| ^{68}Se | 1.6 m | −261 | 1.6 m | −450 | 36 s | −0.97 |

channels of (n, γ) , (n, p) , (n, α) and their reverse reactions. As for the weak interaction processes, we have added β^- -decays and electron captures by Fuller et al. (1980, 1982). These nuclear data are taken from the data base REACLIB¹. Some reaction rates have been also included in connection to the calculations of nucleosynthesis in novae (Wanajo et al. 1998): the reactions (p, γ) for the nuclei of $^{23,24}\text{Al}$, ^{26}Si , ^{27}P , ^{30}S , $^{31,32}\text{Cl}$, $^{34,35}\text{Ar}$, and ^{35}K are taken from Herndl et al. (1995). Those for ^{25}Mg and ^{25}Al are taken from Iliadis et al. (1996) and the isomeric state of ^{26}Al is separated from the ground state at $T < 4 \cdot 10^8$ K and treated as a different nucleus (Wanajo et al. 1998). We note that the β -decay half life of ^{68}Se in REACLIB is replaced from 1.6 min to 35.5 s (e.g. Horiguchi et al. 1996). Furthermore, we have replaced the rate of $^{13}\text{N}(p, \gamma)^{14}\text{O}$ in the above REACLIB by the new one (Rayet 1998) which includes the new experimental results (e.g. Keiner et al. 1993); this reaction is crucial for the break out from the HCNO cycle. For simplicity, we have not included such a 2p-capture process as suggested by Schatz et al. (1998). To investigate the effects of the Q -values and the reaction rates on the thermal history, we have performed the calculations for three cases as shown in Table 2. For case B, they are taken from Schatz et al. (1998), and for case C, they are from REACLIB. With the above modifications of the nuclear data, numerical computations are carried out in case A and case B by HA85, and in case C we use the updated network of Table 1. Screening factors for the thermonuclear reaction rates are taken from Ogata et al. (1991), and Ichimaru & Ogata (1991). It should be noted that the screening effects play an important role for $\rho \gtrsim 10^7$ g cm $^{-3}$.

It has been known that the amounts of CNO elements in the burning shell affect the thermonuclear history of the flash (e.g. Fujimoto et al. 1987). For example, we have $\Delta M \propto Z_{\text{CNO}}^{-0.5}$ at the ignition and the ignition temperature $T_{\text{ig}} \propto Z_{\text{CNO}}^{1/9}$ (Bildsten 1998). Z_{CNO} ranges from 10^{-2} to 10^{-3} and other heavier elements could be transferred from the companion star. Since these initial abundances are rather uncertain, we assume $X(^1\text{H}) = 0.73$, $X(^4\text{He}) = 0.25$ and $X(^{14}\text{O}) = 0.007$, $X(^{15}\text{O}) = 0.013$ from the β^+ -decay saturated HCNO cycle as was done by HSH: denoted as HCNO in Table 3. We also assume the solar system abundances as an alternative initial composition, since often solar seeds have been adopted to study the nuclear process (e.g. Rembges et al. 1997): they are denoted as Solar in Table 3.

¹ <http://csa5.lbl.gov/~fchu/astro/friedel.html>.

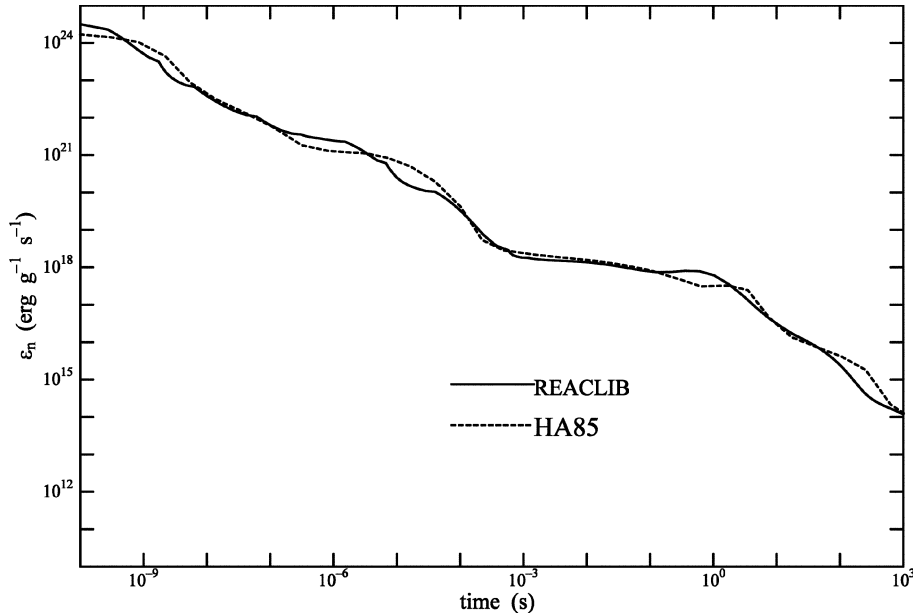


Fig. 1. Comparison of the energy generation rate under the constant temperature $T_9 = 1.5$ and density $\rho = 10^6 \text{ g cm}^{-3}$. Solid line is the results with the use of new rates (REACLIB) and dotted line is those with old rates (HA85).

For all computations, the initial temperature is set to be $1.5 \times 10^8 \text{ K}$; the initial density is obtained from the equation of state. This assumption does not affect the computational results, because T_{max} is attained just after the main nuclear energy is released.

4. Computational results

In Fig. 1, we compare the nuclear energy generation rates under the condition of $T_9 = 1.5$ and $\rho = 10^6 \text{ g cm}^{-3}$ for REACLIB (case C) and HA85 (see also Wormer et al. 1994). We cannot discern the appreciable differences between them: the effects of uncertainties of nuclear data are not clear. This is not the case for X-ray bursts as described below.

According to the spherically symmetric models, to ignite the shell flashes we have $\Sigma_8 \gtrsim 1.2$ (Hanawa & Fujimoto 1982). However, the parameters cannot be specified well from the one-zone model, because the ignition conditions depend sensitively on dM/dt , helium abundances, and Z_{CNO} . Therefore, we have selected the following parameter sets of the pressure and the surface gravity: $(\log P, \log g_s) = (22.75, 14.5), (22.9, 14.75), (23, 14.25), (23, 14.5), \text{ and } (23, 14.75)$, respectively; these are the cases with an appreciable amount of hydrogen left unburnt after the flash (see HSH) which are relevant to the present investigation. It is noted that in these ranges of parameters, we see that $9 \times 10^{-13} \lesssim \Delta M/M_\odot \lesssim 4 \times 10^{-12}$ for $R = 10 \text{ km}$.

Let us study the effects of uncertainties of the nuclear data on the shell flash using the typical parameter $(\log P, \log g_s) = (23, 14.75)$ with the initial composition HCNO. Before the stage of the flash, the HCNO cycle is regulated by intervening β^+ -decays; the energy generation rate is governed by the stable hydrogen burning of $\varepsilon_{\text{H}} \simeq 10^{14} (Z_{\text{CNO}}/0.02) \text{ ergs g}^{-1} \text{ s}^{-1}$. Then, the shell flash begins to occur as is seen from Fig. 2. Note that the scale of the lower abscissa corresponds to cases A and B, and that of the upper one corresponds to case C. The nuclear

process over a shell flash can be classified in three categories. For $T_9 \lesssim 0.3$, HCNO cycle operates rather slowly. Beyond $T_9 \gtrsim 0.3$, break out from HCNO cycle occurs very rapidly through the reactions of $^{14}\text{O}(\alpha, p)^{17}\text{F}$ and $^{15}\text{O}(\alpha, \gamma)^{19}\text{Ne}$ which trigger the *explosive combined hydrogen and helium burning*. The ignition of the flash leads to the first sharp peak in the energy generation rate as seen in Fig. 2 which shows the formation of the iron peak elements. The second peak corresponds to the formation of ^{56}Ni . Transition from ^{56}Ni to ^{64}Ge makes the third peak; the peaks in cases A and B is wider compared with case C due to the effects of the different Q -values for ^{64}Ge . A small difference between cases A and B is seen for $t \sim 350\text{--}360 \text{ s}$ because the transition of the abundance peak from ^{64}Ge to ^{68}Se affects the decrease in the energy generation. When $T_{9p} \gtrsim 1$, the rp-process proceeds appreciably beyond ^{56}Ni . The nucleosynthesis depends on the Q -value of the waiting nuclei; The nuclei shown in Table 2 play an important role to determine the rp-process path. In particular, the Q -value of $^{68}\text{Se}(p, \gamma)^{69}\text{Br}$ is not yet known; proton drip line along some key nuclei is uncertain. Schatz et al. (1998) assumed the Q -value of -450 keV and described the uncertainty in Q -values of (p, γ) reactions.

From Fig. 3, once the breakout from the HCNO cycle occurs, the nuclear flash leads to the peak temperature T_p . The typical changes in the temperature and the density can be seen in Fig. 4. However, comparison of Figs. 5 and 6 reveals that new reaction rates change the time variation of compositions significantly; breakout from the HCNO cycle is appreciable for case C before the depletion of $^{14,15}\text{O}$. Consequently, before the shell flash begins the rp-process proceeds up to the formation of ^{40}Ca and ^{52}Fe through successive (p, γ) and (α, p) reactions changing the nucleosynthesis path by β^+ -decays; this leads to steep rise in temperature during the flash phase due to abundant seed heavy nuclei as seen in Figs. 3 and 6. Then, compared with case B or HSH, more nuclear energy has been released when the flash begins; higher peak temperature is attained as illus-

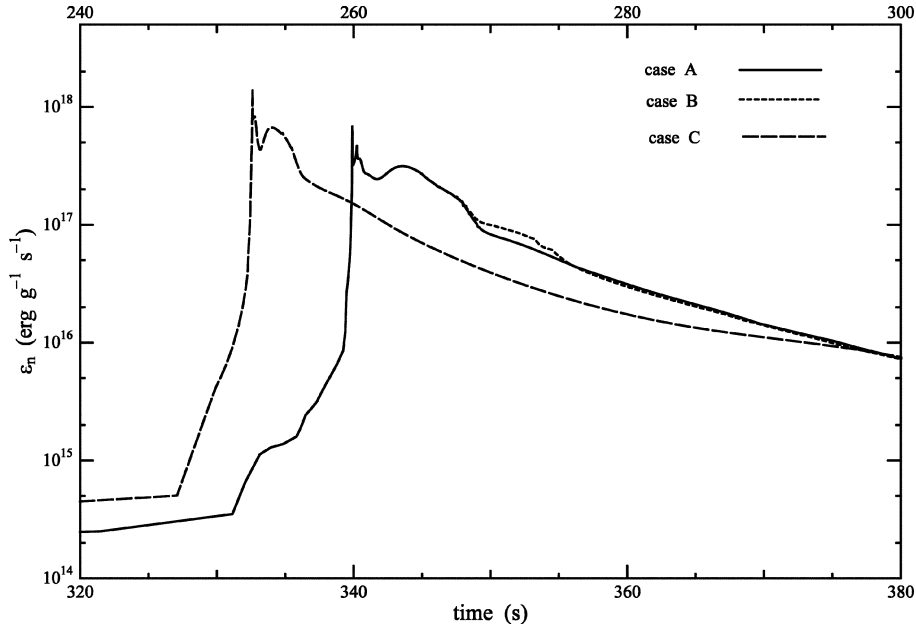


Fig. 2. Comparison of the energy generation rate during the flash for the models of $\log P = 23$, $\log g_s = 14.75$. Solid line: case A, dotted line: case B (scale of the lower abscissa), and dashed line: case C (scale of the upper one).

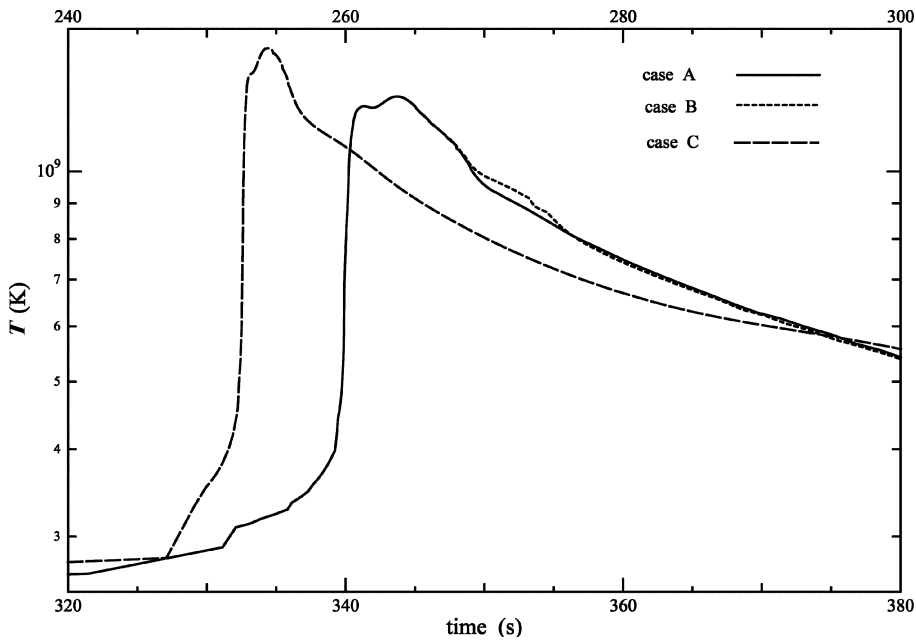


Fig. 3. Time variation of the temperature during the flash for the same models as in Fig. 2.

trated in Fig. 4: the locus extends to lower density for case C. The effects of the Q -values are clear as inferred from Table 2. For case A, the waiting point results from the decays of ^{64}Ge and ^{68}Se . For case B, decay of ^{68}Se corresponds to the final waiting point. For case C, decay of ^{72}Kr might lead to a new waiting point as suggested by Mathews (1991). The large differences in the Q -values for $^{64}\text{Ge}(p, \gamma)^{65}\text{As}$ affect the degree of the decrease in the tails as seen in Figs. 2 and 3. When the temperature decreases down to $2 \cdot 10^8$ K, only weak interactions are active. As is seen from Tables 3 and 4, the *final* products at this temperature depend significantly on the nuclear data, which could affect the modeling of type I X-ray bursts in especially 10 minutes intervals.

We should note that since the thermal history is crucial to X-ray bursts as is shown in Figs. 2, 3, and 4, the condition of the constant temperature and density or an artificial assumption of “adiabatic expansion” (e.g. Rembges et al. 1997) is inadequate to investigate the nuclear process during the shell flashes.

We can examine how the shell flashes are affected by the initial compositions as shown in Table 3. Since the solar seeds have more heavy elements of $Z > 8$, the elapsed time to the peak temperature is shorter than that for HCNO by an order of magnitude. However, the values of the peak temperature and the amounts of the final products are similar for both initial compositions though hydrogen is rather consumed for the initial Solar abundances by the seed nuclei. Therefore, as far as the

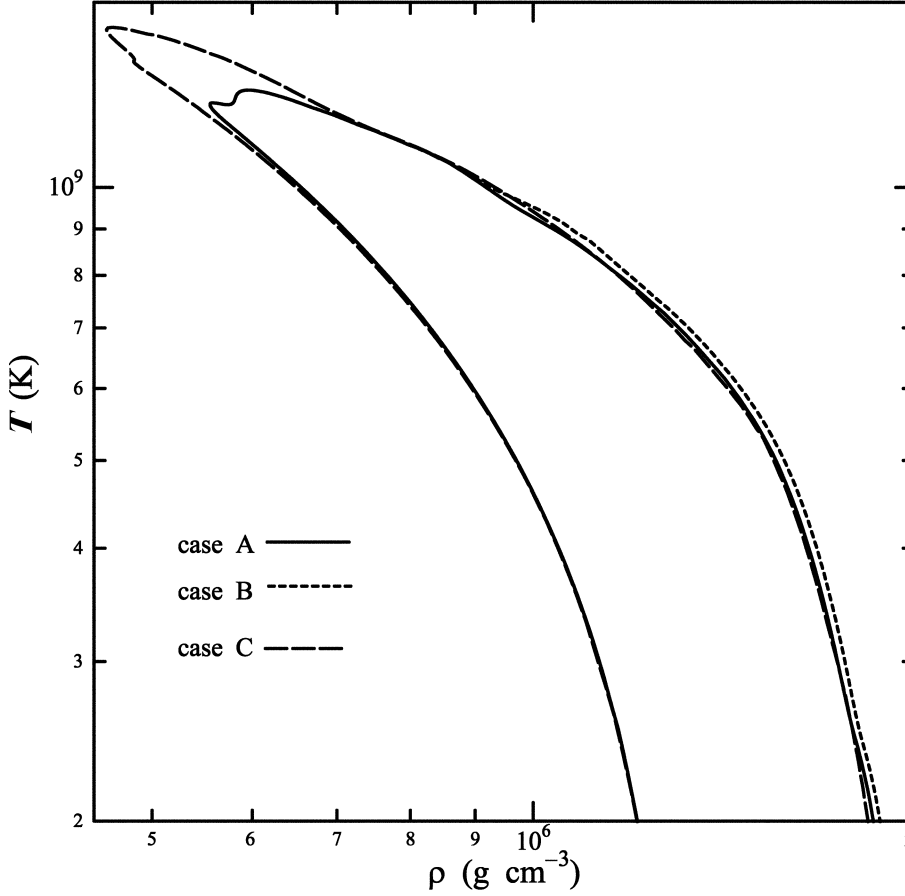


Fig. 4. Same as Fig. 2 but for the changes of the temperature and the density during the flash.

simple one zone model is concerned, it is reasonable to adopt the initial compositions as HCNO.

The radiative luminosity is given as $L_{\text{rad}} = 4\pi R^2 \Sigma \varepsilon_{\text{rad}}$, where Σ and R are fixed in our sequence of calculations. Then, light curve of our model is characterized in terms of ε_{rad} as shown in Fig. 7. We should note that profiles of the light curves are affected significantly by the different nuclear data. On the other hand, the Eddington luminosity L_{Edd} in the local frame is given by

$$\begin{aligned} L_{\text{Edd}} &= \frac{4\pi c G M_t}{\kappa} \left(1 - \frac{2GM_t}{rc^2}\right)^{-1/2} \\ &= \frac{2.5 \cdot 10^{38}}{1 + X} \text{V ergs s}^{-1}. \end{aligned} \quad (10)$$

With the use of the corresponding Eddington luminosity $\varepsilon_{\text{Edd}} = cg_s/(\kappa\Sigma)$, we could obtain

$$\frac{L_{\text{rad}}}{L_{\text{Edd}}} = \frac{4a}{3} \frac{T^4}{\Sigma g_s} = \frac{T_9^4}{\Sigma_8 g_{14}}. \quad (11)$$

It appears that $L_{\text{rad}} > L_{\text{Edd}}$ if $T_9 > 1$ (see Tables 2 and 4). However, it should be noted that the condition of $T_{\text{max}} > 10^9$ K is satisfied around the bottom of the burning shell in the actual situation: in evaluating L_{rad} , R would be the radius of the photosphere and κ will be different layer by layer inside the neutron star atmosphere. Then, L_{rad} remains below L_{Edd} as long as both the spherically symmetric configuration (Hashimoto et al. 1993)

and hydrostatic equilibrium are assumed (see also Ebisuzaki et al. 1983).

In Table 4 we presented the final abundances with the use of the nuclear data of case C for several sets of parameters which had been performed by HSH. We can see that the final products depend on the peak temperature and the radiative energy loss rate; contrary to the results of HSH, if $\log g_s \lesssim 14.5$ and $T_{9p} \gtrsim 1.5$, the main final products are not ^{68}Ge but ^{74}Se and ^{74}Kr . This indicates that the waiting point is beyond ^{68}Se and the flow of abundances will be beyond Kr isotopes. However it must be noted that the final products and/or the amount of the fuel left after the flash depend on both the Q -value of $^{68}\text{Se}(p, \gamma)^{69}\text{Br}$ seen in Table 3 and the radiative energy loss rate which may be too simplified for our one zone model.

5. Discussion and conclusions

Using a simple but crucial model of the thermonuclear flash on accreting neutron stars, we have shown that the nuclear data near the proton drip line affect the rp-process significantly: the energy generation rate (peak temperature) as shown in Figs. 2, 3 and 4. The amounts of the fuel left after the flash (final products) are shown in Figs. 5 and 6. The *final* products are summarized in Tables 3 and 4. As a consequence, the profile of the light curve must be affected also as shown in Fig. 7. Compared with HSH, break out from the HCNO cycle is so rapid that iron peak elements have been produced before the flash. Contrary to the

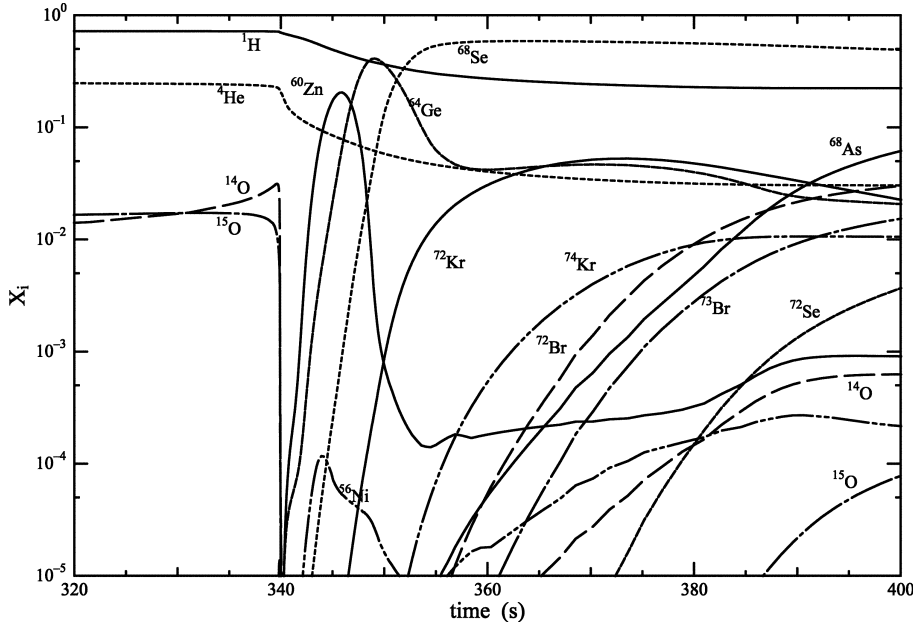


Fig. 5. Changes of mass fractions during the flash. Case B of $\log P = 23$, $\log g_s = 14.75$.

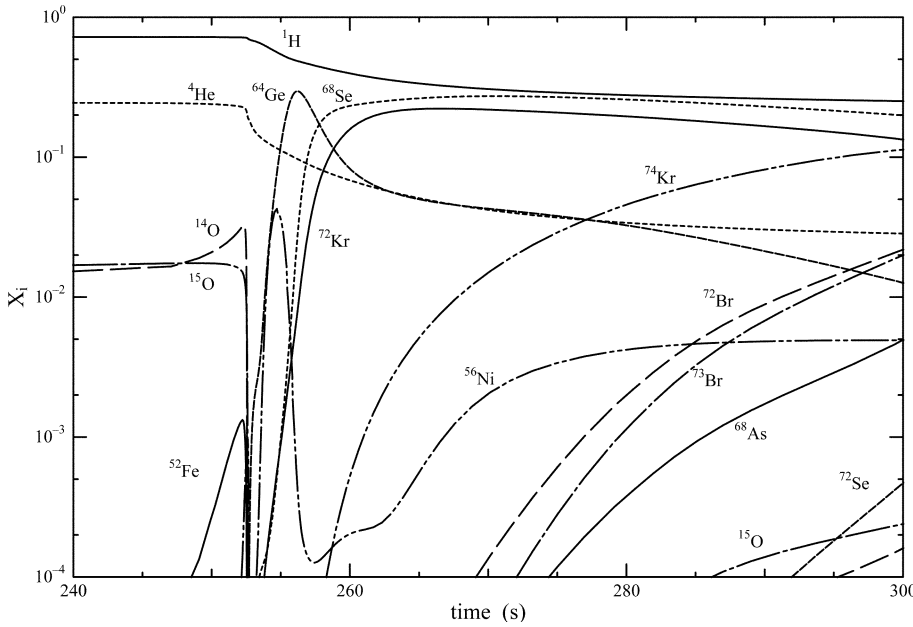


Fig. 6. Same as Fig. 5 but for case C.

large differences in the rp-process attributed to the various nuclear data, the differences are quantitatively very small between independent calculations of the explosive nucleosynthesis in supernovae (e.g. Hashimoto et al. 1989, Thielemann et al. 1990) because the supernova nucleosynthesis proceeds under the condition of approximately nuclear statistical equilibrium.

It is noted that, since our network is limited to Kr isotopes, we should extend it to include the nuclei of $Z > 36$ for the high temperature cases with $P \gtrsim 10^{23}$ dyn cm^{-2} as pointed out by Schatz et al. (1998) though the flow beyond Kr depends on the Q -value of waiting nucleus ^{68}Se ; only in the deepest accreted layer the rp-process beyond Kr would proceed appreciably (see Fig. 5 in Fujimoto et al. 1987). Therefore, it is highly

needed to determine the proton drip line from Ge to Kr isotopes (Mohar et al. 1991, Henncheck et al. 1994, Blank 1995).

While our one zone model represents rather well the flash phase, convection must be actually taken into account. Fujimoto et al. (1987) demonstrated the importance of the mixing process to explain bursts of very short intervals like 10 minutes X-ray bursts (e.g. Murakami et al. 1980). They used spherically symmetric evolutionary code, and the helium abundances averaged in the burning shell are assumed with the use of an approximate network of the previous version of HSH. It should be noted that the mixing process is still very uncertain. Therefore, one zone approach is still very useful to see how the rp-process will be affected by the change of the nuclear data and other physical

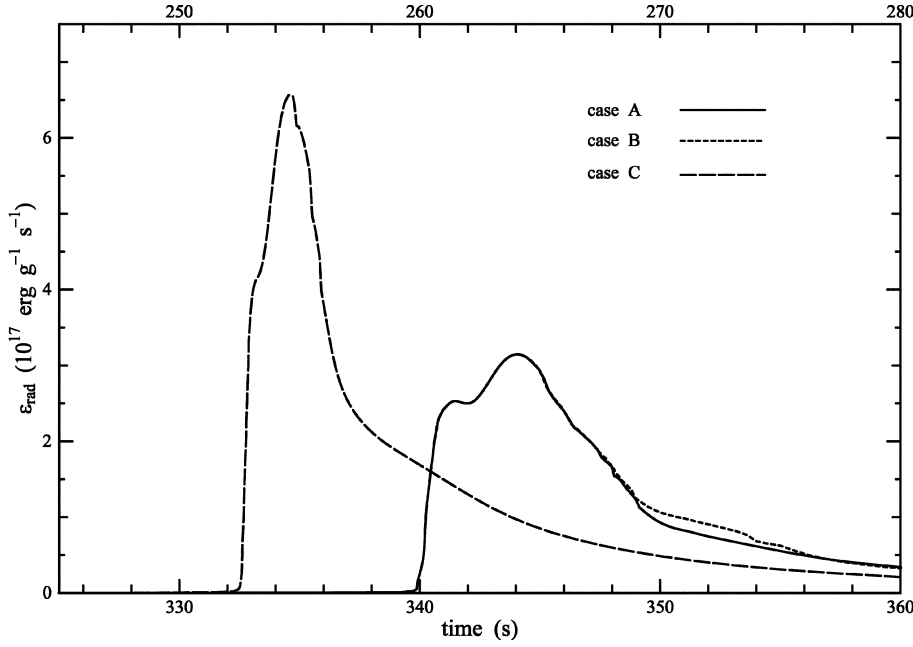


Fig. 7. Light curves with the same parameters as in Fig. 2.

Table 3. Final mass fractions after the shell flashes of $\log P = 23$, $\log g_s = 14.75$ when $T_9 = 0.2$ with the different initial compositions and Q -values. T_{9p} is the peak temperature in 10^9 K and t_p is the elapsed time until the peak temperature is attained. HCNO means the initial abundances of the β^+ -decay saturated HCNO cycle. Solar means the solar system abundances.

| nucleide | HCNO | | Solar | | HCNO | Solar |
|------------------|----------|----------|----------|----------|----------|----------|
| | case A | case B | case A | case B | case C | |
| T_{9p} | 1.28 | 1.28 | 1.29 | 1.29 | 1.50 | 1.51 |
| t_p | 3.44(+2) | 3.44(+2) | 3.90(+1) | 3.90(+1) | 2.54(+2) | 7.49 |
| ^1H | 2.35(-1) | 2.23(-1) | 2.01(-1) | 1.87(-1) | 2.46(-1) | 2.02(-1) |
| ^4He | 3.08(-2) | 3.05(-2) | 3.01(-2) | 2.98(-2) | 2.74(-2) | 2.66(-2) |
| ^{56}Ni | 1.43(-4) | 1.66(-4) | 1.70(-4) | 1.98(-4) | 3.15(-3) | 3.96(-3) |
| ^{64}Zn | 1.37(-1) | 1.62(-2) | 1.65(-1) | 2.20(-2) | 3.72(-3) | 5.09(-3) |
| ^{64}Ga | 5.66(-2) | 7.13(-3) | 6.64(-2) | 9.60(-3) | 2.61(-3) | 4.24(-3) |
| ^{65}Ga | 1.50(-2) | 7.48(-3) | 1.61(-2) | 9.03(-3) | 2.22(-3) | 3.00(-3) |
| ^{64}Ge | 4.06(-3) | 5.45(-4) | 4.19(-3) | 6.43(-4) | 3.37(-4) | 6.60(-4) |
| ^{68}Ge | 2.49(-1) | 3.38(-1) | 2.52(-1) | 3.57(-1) | 1.17(-1) | 1.27(-1) |
| ^{68}As | 1.23(-1) | 1.77(-1) | 1.22(-1) | 1.87(-1) | 6.07(-2) | 7.90(-2) |
| ^{68}Se | 2.70(-2) | 4.07(-2) | 2.51(-2) | 4.05(-2) | 9.87(-4) | 1.81(-3) |
| ^{72}Se | 3.63(-2) | 5.34(-2) | 3.46(-2) | 2.68(-3) | 1.31(-1) | 1.38(-1) |
| ^{72}Br | 1.80(-3) | 2.92(-3) | 1.55(-3) | 2.68(-3) | 1.45(-2) | 1.97(-2) |
| ^{73}Br | 8.15(-3) | 1.23(-2) | 7.09(-3) | 1.13(-2) | 7.83(-2) | 8.69(-2) |
| ^{74}Kr | 5.12(-3) | 7.33(-3) | 4.14(-3) | 6.10(-3) | 9.42(-2) | 8.94(-2) |

inputs. Though the detailed multi-dimensional hydrodynamical calculation would be desirable, even the spherical calculation of stellar evolution should be highly necessary to see the effects of uncertainties of nuclear data. Then, approximate network which simulates nuclear energy generation rates should be employed in realistic calculations as is done by Fujimoto et al. (1987).

Recent observations of quasi-periodic oscillations may constrain the mass and radius of neutron stars. For example, analyzing the LMXB 4U 1636-536, Kaaret et al. (1997) suggested that the mass and the radius of the neutron star are around $2.0 M_\odot$ and 9.0 km, respectively, which is nearly compatible with the maximum state derived from the equation of state by Friedman

& Pandharipande (1981). Then, we have $\log g_s = 14.75$ with $V = 1.7$. A neutron star of $M_t = 1.1 M_\odot$ and $R = 10$ km has $\log g_s = 14.25$ with $V = 1.22$ which state is reproduced by the equation of state AV14+UVII by Wiringa et al. (1988). Taam et al. (1996) adopted a star of $M_t = 1.4 M_\odot$ and $R = 9.1$ km; $\log g_s = 14.5$ with $V = 1.35$. Therefore, our parameters are within the range of more realistic X-ray burst models.

Related to the rp-process, Chakrabarti et al. (1987) pointed out the possibility inside a thick accretion disk around a stellar mass black hole. Recent calculations of nucleosynthesis inside thick accretion disks have suggested that significant nuclear processing would occur if a viscosity is low (e.g. Arai & Hashimoto

Table 4. *Final* mass fractions after the shell flashes for calculated models with the HCNO initial compositions. All models are computed by case C.

| $\log P$ | 22.75 | 22.90 | 23.00 | 23.00 | 23.00 |
|------------------|----------|----------|-----------|----------|----------|
| $\log g_s$ | 14.50 | 14.75 | 14.25 | 14.50 | 14.75 |
| T_{9p} | 1.41 | 1.38 | 1.91 | 1.75 | 1.50 |
| t_p | 5.24(+2) | 1.29(+3) | 1.44(+2) | 1.52(+2) | 2.54(+2) |
| ^1H | 1.77(-1) | 1.66(-1) | 3.22(-1) | 2.88(-1) | 2.46(-1) |
| ^4He | 3.73(-2) | 3.63(-2) | 1.46(-2) | 1.82(-2) | 2.74(-2) |
| ^{56}Ni | 9.49(-3) | 1.32(-2) | 1.72(-5) | 4.18(-4) | 3.15(-3) |
| ^{64}Zn | 2.09(-2) | 2.46(-2) | 2.09(-4) | 3.67(-4) | 3.72(-3) |
| ^{64}Ga | 1.33(-2) | 2.43(-2) | 4.88(-10) | 3.85(-4) | 2.61(-3) |
| ^{65}Ga | 8.08(-3) | 1.25(-2) | 5.53(-6) | 3.85(-4) | 2.22(-3) |
| ^{64}Ge | 1.56(-3) | 4.56(-3) | 7.32(-16) | 7.74(-5) | 3.37(-4) |
| ^{68}Ge | 1.67(-1) | 1.98(-1) | 1.95(-3) | 1.30(-2) | 1.17(-1) |
| ^{68}As | 7.87(-2) | 1.49(-1) | 4.45(-10) | 1.01(-2) | 6.07(-2) |
| ^{69}As | 2.31(-2) | 2.98(-2) | 5.49(-5) | 5.80(-3) | 2.02(-2) |
| ^{68}Se | 1.07(-3) | 4.70(-3) | 9.81(-18) | 3.40(-4) | 9.87(-4) |
| ^{72}Se | 1.17(-1) | 1.10(-1) | 2.96(-3) | 2.64(-2) | 1.31(-1) |
| ^{73}Se | 9.23(-2) | 4.62(-2) | 1.08(-2) | 6.01(-2) | 1.14(-1) |
| ^{74}Se | 2.23(-3) | 3.76(-4) | 4.06(-1) | 5.79(-3) | 2.39(-3) |
| ^{72}Br | 1.12(-2) | 2.02(-2) | 1.17(-14) | 4.80(-3) | 1.45(-2) |
| ^{73}Br | 5.82(-2) | 4.46(-2) | 4.07(-8) | 5.74(-2) | 7.83(-2) |
| ^{74}Br | 2.71(-2) | 5.94(-3) | 1.06(-1) | 9.43(-2) | 3.07(-2) |
| ^{74}Kr | 7.87(-2) | 2.25(-2) | 6.77(-3) | 3.66(-1) | 9.42(-2) |
| ^{75}Kr | 1.46(-3) | 2.78(-4) | 4.92(-6) | 1.72(-2) | 1.55(-3) |

1992, 1995); it may be promising for the rp-process to occur if hydrogen is mixed into the hot interior material. Though the disk model is still rather uncertain, it is worth while to investigate the nucleosynthesis using another model like advection dominated disk; if it occurs, some accretion disks could give an important site of nucleosynthesis even in the early stage of the universe.

Finally, we want to stress the difference of the available reaction rates. We employed REACLIB and compared the results with the old rates, many of which seem to be still surviving. The database of another reaction rates (HW92)² in which reaction rates are tabulated in specified temperature grids has been mostly adopted in our cases A and B except for some reactions in Caughlan & Fowler (1988). It must be noted that if we compare individual rates in two databases, many of them have significant deviations in the temperature range of $0.1 \lesssim T_9 \lesssim 10$ which is relevant in the present investigations. In particular, as the temperature becomes higher, say, $T_9 \gtrsim 1.0$, differences become larger; in part due to the different treatment of the level density. Let us evaluate the ratio f of the reaction rate given by REACLIB to HW92. For example, one has $f = 0.09$ for $^{68}\text{Se}(p, \gamma)^{69}\text{Br}$ in $T_9 = 1.5$, and $f = 0.3$ for $^{56}\text{Ni}(p, \gamma)^{57}\text{Cu}$ in $T_9 = 1.0$. Even for the lower temperature, $f = 61$ for $^{17}\text{F}(p, \gamma)^{18}\text{Ne}$ and $f = 76$ for $^{13}\text{N}(p, \gamma)^{14}\text{O}$ in $T_9 = 0.5$. However, it must be noted that $f = 2.5$ for European Compilation instead of REACLIB for $^{13}\text{N}(p, \gamma)^{14}\text{O}$ (Rayet 1998, see also the experimental value by Kiener et al. 1993). Though the effects of these dif-

ferences on X-ray burst phenomena are not always clear, we should be careful of the uncertainty of reaction rates.

Acknowledgements. We thank Dr. M. Rayet to have kindly informed us of the up-to-date reaction rate of $^{13}\text{N}(p, \gamma)^{14}\text{O}$. Thanks are given to Dr. K. Kubono for discussion on the nuclear data. M. H. and O. K. are grateful to Mr. N. Noda for his help to check some computational results. We thank the referee, Dr. A. Y. Potekhin, for useful remarks and comments.

References

- Arai K., Hashimoto M., 1992, A&A 254, 191
Arai K., Hashimoto M., 1995, A&A 302, 99
Bildsten L., 1998, In: Alpar A., Buccheri R., van Paradijs J. (eds.) Proc. NATO/ASI, The Many Faces of Neutron Stars. Kluwer, Dordrecht, in press
Brown G.E., Bethe H.A., 1994, ApJ 423, 659
Chakrabarti S.K., Jin L., Arnett W.D., 1987, ApJ 313, 674
Blank B., 1995, Phys. Rev. Lett. 74, 4611
Fowler W.A., Caughlan G.R., Zimmerman B.A., 1975, ARA&A 13, 69
Caughlan G.R., Fowler W.A., Zimmerman B.A., 1985, At. Data Nucl. Data Tables 32, 197
Ebisuzaki T., Hanawa T., Sugimoto D., 1983, PASJ 35, 17
Friedman B., Pandharipande V.R., 1981, Nucl. Phys. A361, 502
Fujimoto M., Hanawa T., Miyaji S., 1981, ApJ 247, 267
Fujimoto M., Sztajno M., Lewin W.H.G., van Paradijs J., 1987, ApJ 319, 902
Fuller G.M., Fowler W.A., Newman M., 1980, ApJS 42, 447
Fuller G.M., Fowler W.A., Newman M., 1982, ApJS 48, 279
Hanawa T., Fujimoto M., 1982, PASJ 34, 495
Hanawa T., Sugimoto D., Hashimoto M., 1983, PASJ 35, 491 (HSH)
Harris M., Fowler W.A., Caughlan G.R., Zimmerman B.A., 1983, ARA&A 13, 69
Hashimoto M., Hanawa T., Sugimoto D., 1983, PASJ 35, 1
Hashimoto M., Arai K., 1985, Phys. Rep. Kumamoto Univ. 7, 47 (HA85)
Hashimoto M., Nomoto K., Shigeyama T., 1989, A&A 210, L5
Hashimoto M., Eriguchi Y., Arai K., Müller E., 1993, A&A 268, 131
Henncheck M., et al., 1994, Phys. Rev. C50, 2214
Herndl H., et al., 1995, Phys. Rev. C52, 1078
Horiguchi T., Tachibana T., Katakura J., 1996, Chart of the Nuclides. Nuclear Data Center, JAERI, Tokai, Ibaraki
Iliadis C., et al., 1996, Phys. Rev. C53, 475
Ichimaru S., Ogata S., 1991, ApJ 374, 647
Kaaret P., Ford E.C., Chen K., 1997, ApJ 480, L27
Kiener, et al., 1993, In: Käppeler F., Wisshak K. (eds.) Proc. Nuclei in the Cosmos. IOP publishing, p. 317
Lewin W.G., van Paradijs J., R.E. Taam, 1993, Space Sci. Rev. 62, 223
Mathews G.J., 1991, Nat, 351, 348
Mohar M.F., et al., 1991, Phys. Rev. Lett. 66, 1571
Murakami T., et al., 1980, PASJ 32, 543
Nomoto K., Hashimoto M., 1988, Phys. Rep. 163, 13
Ogata S., Iyetomi H., Ichimaru S., 1991, ApJ 372, 259
Rayet M., 1998, private communication from European Nuclear Astrophysics Compilation of Reaction Rates, to be published in Nucl. Phys.
Rembges F., et al., 1997, ApJ 484, 412
Slattery W.L., Doolen G.D., De Witt H.E., 1982, Phys. Rev. A26, 2255
Smale A.P., 1998, ApJ 498, L141

² http://csa5.lbl.gov/~fchu/astro/hw92_1.html.

- Schatz H., et al., 1998, Phys. Rep. 294, 167
Strohmayer T.E., et al., 1998, ApJ 498, L135
Taam R.E., 1985, Ann. Rev. Nucl. Part. Sci. 35, 1
Taam R.E., Woosley S.E., Lamb D.Q., 1996, ApJ 459, 271
Thielemann F.-K., Hashimoto M., Nomoto K., 1990, ApJ 349, 222
Thielemann F.-K., 1997, FTP site in quasar.physik.unibas.ch
Wallance, R.K., Woosley S.E., 1981, ApJS 45, 389
Wanajo S., Hashimoto M., Nomoto K., ApJ submitted
Wiringa R.B., Fiks V., Fabrocini A., 1988, Phys. Rev. C38, 1010
Wormer L.V., Gorres J., Iliadis C., Wiesher M., Thielemann F.-K., 1994, ApJ 432, 1994
Woosley S.E., Fowler W.A., Holmes J.A., Zimmerman B.A., 1975, OAP-422, Caltech, unpublished
Woosley S.E., Fowler W.A., Holmes J.A., Zimmerman B.A., 1978, At. Data Nucl. Data Tables 32, 197
Yakovlev D.G., Shalybkov D.A., 1989, Sov. Sci. Rev. E: Astrophys. Space Phys. Rev. 7, 313